Bionic Body Wave Control for an Eel-Like Robot Based on Segmented Soft Actuator Array

Ronghao Dang[1], Haisong Gong[1], Yuxin Wang[1], Tianyi Huang[1], Zhuofan Shi[1],
Xinwen Zhang[2], Yunfeng Wu[1], Yi Sun[3], Peng Qi[1]

1. Tongji University, Shanghai 200092, China
E-mail: pqi@tongji.edu.cn

2. University of Twente, 7522 NB Enschede, Netherlands
E-mail: x.zhang-15@student.utwente.nl

3. Australian Center for Field Robotics and Sydney Institute for Robotics and Intelligent Systems,
University of Sydney, Sydney, New South Wales, 2006, Australia
E-mail: yi.sun1@sydney.edu.au

Abstract: Using body wave to swing forward is the most common propulsion method for underwater creatures, which can achieve flexible swing and multi-directional steering. Related robotics researches in recent years employed rigid structure and hinge connection to build the entire swing body, which were driven by conventional motors. However, soft robotics provides an alternative to make the robot behave like a bionic fish in terms of swing flexibility, actuation and efficiency. In this article, the authors develop the entire eel-like fish with a fully soft flexible body, which is composed of four fiber-reinforced, bidirectionally bending, fluidic elastomer actuators (FEAs) as its tail. This robotic fish tail has multiple segments connected in series with different waveforms to make the overall fish tail exhibit fluctuating forward performances. The FEA uses the typical dual-chamber configuration, and PWM sine wave signals are utilized to effectively control such a hydraulic mechanism. With experiments, the swing of each tail section is tested, and various factors with respect to the swing frequency and amplitude are studied. The results illustrate the feasibility and superiority of the proposed body wave control method.

Key Words: body wave control, soft robotic fish, FEAs

1 Introduction

Bionic fish is a popular research embodiment in the field of soft robotics. Robotic fish can achieve underwater exploration and help humans explore the environment beneath the surface like among other fish and underwater creatures. Generally, the robotic fish is equipped with detection sensors to collect information in the river water, such as, finding a variety of water pollutants - fuel leaked from ships or other chemicals, and drawing a 3D pollution map of the river.

As a cutting-edge robotic technique, soft robots are known for their simple-design, high-performance and low-cost. Developing a soft fish-shaped robot only requires three steps, i.e., design, fabrication and control. There are sufficient off-shelf results for these three steps of soft robotics. Traditional soft robot design is inseparable from computer-aided design (CAD) software, but Marchese *et al*. [1] and Tolley *et al*. [2] used an alternative 3D moulding technology, which provides more detailed information and make the model more realistic. Besides, Lipson *et al*. [3] designed an automated algorithm to design soft robots, and Hiller *et al*. [4] used a custom finite element analysis software (VoxCAD) to generate soft robots, which can use materials with a wide range of moduli and optimize the design of soft robots through evolutionary algorithms.

In terms of fabrication, there are many advanced fabrication methods for novel soft actuator formats [5–7]. Lipson *et al*. in [8] utilized a composite 3D printing technology to build soft robots. Cham *et al*. [9] used Shape Deposition Manufacturing (SDM) to achieve the same effect, and Xia *et al*. [10] also developed soft lithography technology to solve this problem.

The control of soft robots over the years have evolved. Brown *et al*. [11] realized the picking and dropping operations of soft robots without knowing the exact shape and precise position of the object being grasped. Marchese *et al*. [12] confirmed that the use of jet-driven cylinders to achieve control has continuous adjustability and pressurization variability. Napp *et al*. [13] realized a passive valve with memory to actuate multiple soft robot actuators through a single controlled pressure source. His research also realized controlling pneumatic robots without electronic control signals.

In summary, the technology of design, fabrication and control of general soft robots is already mature, but for soft robotic fish, related technologies still needs to be investigated.

The soft bionic fish developed by Katzschmann *et al*. [14] for underwater exploration is the most complete bionic fish robot at present. They integrated all aspects such as drive, energy, sensing, control and communication into their robot. The whole fish is divided into two parts, one is the electronic control room, and the other is the driving actuator. As a representative of the semi-soft robotic fish, their main contribution is to provide a new form of close exploration of underwater life. The soft robotic fish can be sensitive to the tracks of underwater life, equipped with cameras and remote-control systems. However, controlling the fish remotely is a big issue. Because water absorbs most electromagnetic radiation, the widely used communication equipment on land, such as Wi-Fi, Bluetooth, etc., is difficult to work under the water. And the existing underwater communication equipment is too big for fish to carry. Therefore, Robert *et al*. designed an ultrasonic wave generator and re-

This work is supported by the National Natural Science Foundation of China under Grant 51905379; Shanghai Science and Technology Development Funds (20QC1400900).

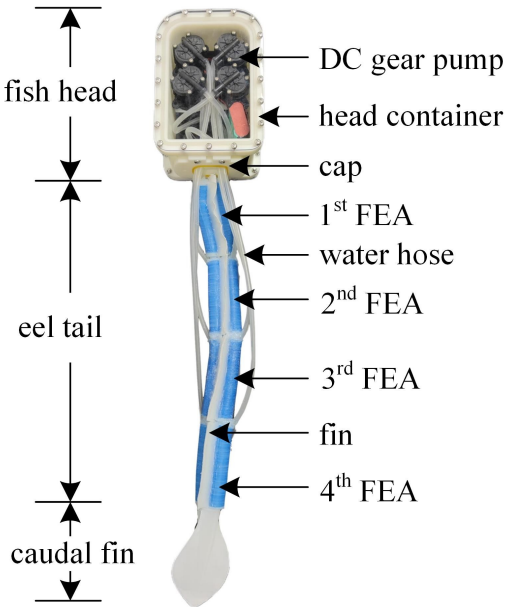

Fig. 1: Overlook of the proposed soft eel-liked robotic fish.

ceiver to realize real-time underwater communication by using self-made communication and coding protocols, which greatly reduced the volume of underwater communication equipment and provided the basis for controlling the underwater soft robotic fish.

The soft robotic octopus developed by Wehner *et al.* [15] is a representative example of soft-bodied underwater fish, and it is the first fully soft robot capable of continuously generating sequential motion. The energy supply, controller, reaction chamber and actuator of the whole octopus are softened by making full use of the soft material, and the octopus can be controlled to oscillate the tentacle movement. This soft octopus mainly used H_2O_2 as soft energy. Since H_2O_2 can be decomposed to produce pollution-free oxygen and hydrogen, it is the optimal choice of soft energy source for general soft robots. And the controller making use of microfluidic technology, completely got out of the limit of power control. The liquid circuit was simulated into the oscillator, on/off valve, check valve and other basic components. Finally, catalyzed by Pt in the reaction chamber, the gas generated by H_2O_2 reaction drives the FEAs to realize the lifting and lowering of octopus feet.

Zhang *et.al.* [16] mainly improved the control algorithm of soft robotic fish. They achieved three degrees of freedom by adjusting the direction of their pectoral and caudal fins. The earliest dynamic angle control method was a linear model with undetermined parameters. Later, in the early 21st century, a central pattern generator (CPGS) control network [17] was proposed to adjust the state of each degree of freedom individually. Zhang *et al.* designed a composite controller to adjust the amplitude of pectoral fins to track the expected pitch angle, and combined with Radial Basis Function (RBE) neural network, proposed an adaptive controller to estimate the undetermined parameters. Feng *et al.* [18] also established a new type of soft robotic fish that can drive its head to swim in shallow waters by swinging its tail. There was plenty of space inside the head, which can accommodate various sensors for underwater detection.

In this paper, a soft eel-like robotic fish capable of operating in water is designed, fabricated and controlled. As depicted in Fig. 1, this eel-like soft robot comprises the head, eel tail and caudal fin. The head is a 3D-printed container mainly inside with an Arduino board for control and four gear pumps for hydraulic actuation. The tail part of the eel consists of four FEAs, each containing two chambers and a dorsal fin, and each chamber is connected to a pump through a water hose. Water from one chamber is pumped to the other to make the fish's tail actuators bend. Combining four FEAs, the soft robotic eel shows a smooth swimming posture under the control of sinusoidal waves. The dorsal fin of the fish body is used to increase the area of contact with the water, giving greater force and a significant forward distance for a single swing. The design of the caudal fin on the one hand also increases the contact area with the water. On the other hand, biologically inspired, it makes the shape of the robot more similar to an eel.

The fish body adopts a fully soft structure, which makes it have more flexible and changeable underwater action mode. Compared with the rigid body underwater driver, the soft body structure can perform more bionic underwater movement through body waves. But how to control this infinite degree of freedom soft structure has become a sticking point. We propose a segmented control concept, by using sinusoidal PWM waves to control the swing of each segment of the fish tail, so as to achieve the body wave of the overall fish tail. This method not only simplifies the difficulty of controlling, but also enables more creative movement through the cooperation between the various sections.

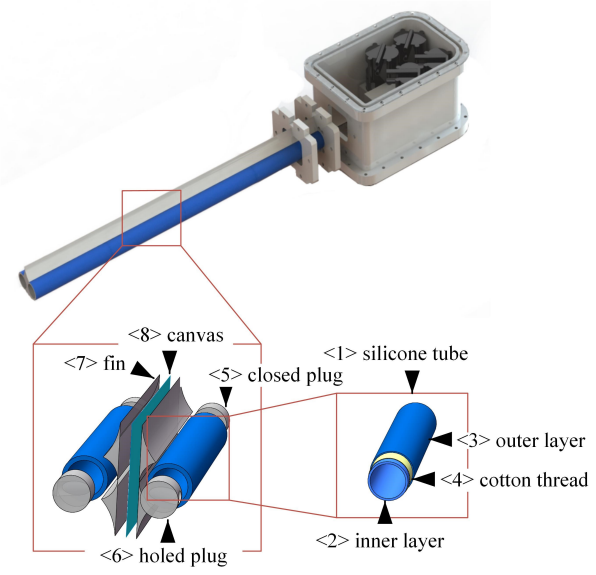

Fig. 2: (a) Scheme of the soft eel-like robot structure and its FEA, which includes ⟨1⟩ two silicone tubes, ⟨5⟩ two closed silicone plugs, ⟨6⟩ two holed silicone plugs, ⟨7⟩ four silicone fins, and ⟨8⟩ a canvas; (b) A silicone tube includes ⟨2⟩ an inner layer, ⟨3⟩ an outer layer, and sandwiched ⟨4⟩ cotton thread that winds the inner layer.

2 Design and Fabrication

In this paper, a bionic soft eel-like robot is designed and fabricated based on FEA method. Such an actuator is completely flexible and it allows bi-directional bending. Each gear pump is driven by a motor module to pump and discharge water continuously, so as to make the soft actuator bend back and forth on both sides, imitating the swing of the eel body in the water.

2.1 FEA Design

The design of the eel-like FEA is illustrated in Fig. 2. This eel-like FEA mainly consists of a pair of cylindrical silicone tubes ⟨1⟩. As shown in Fig. 2, each silicone tube is divided into two layers, where the inner layer ⟨2⟩ is 2 mm thick and the outer layer ⟨3⟩ is 1 mm thick. Cotton thread ⟨4⟩ is applied to wind around the inner layer as fiber reinforcement, and the thickness of thread can be ignored. Fiber reinforcement is to restrain the radial expansion of the silicone tube, so that the silicone tube can only extend axially under compression. The total thickness of the final silicone tube is 3 mm and its length is 100 mm.

A closed silicone plug ⟨5⟩ with a diameter of 7 mm and a thickness of 10 mm is inserted into one end of the silicone tube, while a holed plug ⟨6⟩ of the same size is inserted into the other end, so that the water flow will not leak from both ends when the silicone tube is watered, then the high fluid pressure can be guaranteed, ensuring the actuator to perform sufficient ductility. In order to supply water pressure for the soft actuator, two water hoses are connected with a gear pump and then extended into the tube through the holed plugs. The diameter of the hoses we choose is 6 mm.

The soft robotic fin ⟨7⟩ is a key for the FEA to achieve bending motion. The length of the fin is the same as that of the silicone tube, i.e., 100 mm; the height is 25 mm. In order to make the fin fit well with the cylindrical silicone tube, the cross-section of the fin is designed as an arc with a diameter of 13mm, which intersects another smooth curve, 6.67mm away from the 25mm high line. According to Fig. 2(a), we glue a silicone tube to two robotic fins to fabricate one half of the eel-like body, and then glue two half-bodies together using the silicone adhesive (Smooth-On™ Sil-Poxy) to form a complete FEA, with a layer of canvas ⟨8⟩ sandwiched in the middle. The added canvas increases the adhesion between the two half-bodies, and its stiffness limits the strain of one side of each silicone tube.

When the silicone tube on one side of the FEA is pressurized with water, the silicone tube expands axially due to radial restraint. At the same time, the strain limiting of the canvas layer forces the silicone tube to bend outwards, and eventually the whole FEA to bend to the water filled side. By filling and pumping water to both sides periodically, the fish tail can swing back and forth in a certain frequency.

2.2 Fabrication Process

The eel-like FEA is fabricated entirely by soft lithography [18–21]: two silicone tubes, four silicone plugs and a soft fin, each of them is obtained by casting silicone in the 3D-printed molds.

Ecoflex™ 00-30 is chosen as the silicone material to mold the silicone tubes and the fin. For a silicone tube, firstly, the 2mm-thick inner tube is obtained by casting silicone in the inner-layer mold; then, a winding machine driven by two stepper motors is used to wind cotton thread around the inner layer; finally, the inner tube with fiber reinforcement is placed in the outer-layer mold for secondary casting, to obtain an outer layer with a thickness of 1mm. The structure of the outer-layer mold is similar to that of the inner-layer mold, but the former one's size is slightly larger. In addition, the inner-layer mold is equipped with three central shafts to create fluid channels in the FEA during casting.

The molding material of the silicone plugs is Dragon-Skin™ 30. The silicone adhesion for FEA silicone tubes, silicone plugs and the fin are Smooth-On™ Sil-Poxy.

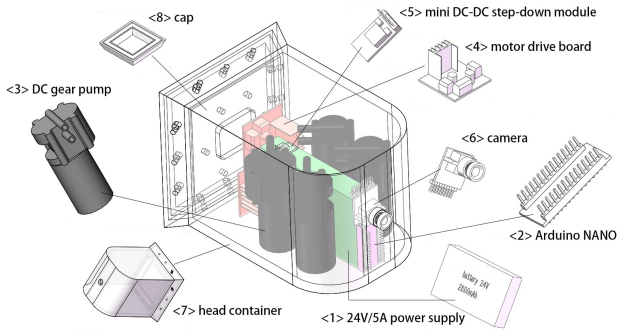

Fig. 3: The decomposition of the robotic eel head, including ⟨1⟩ a 24V/5A power supply, ⟨2⟩ an Arduino NANO board, ⟨3⟩ four gear pumps, ⟨4⟩ two motor drive boards, ⟨5⟩ a mini DC-DC step-down module, and ⟨6⟩ a camera together in ⟨7⟩ the head container with ⟨8⟩ a cap.

2.3 Energy and Control of the FEA

In order to test the performance of FEA, we have equipped the actuator with the energy input and a controller. As shown in Fig. 3, we use a 24V/5A DC power supply ⟨1⟩, an Arduino NANO board ⟨2⟩, four DC gear pump (Zhongchuang Electronics™ ZC-A260) ⟨3⟩, a motor drive board (L298N) ⟨4⟩, a mini DC-DC step-down module ⟨5⟩, and a camera (OV7725) ⟨6⟩ which are together placed in a 3D-printed container ⟨7⟩ with a cap ⟨8⟩ in its back. The function of the step-down module is to step down the 24 V DC power for the Arduino NANO board and the L298N.

3 Drive and Waveform

The design of driving structure and signal waveform is the basis of using body wave control to move the soft robot. The soft fish in this article uses the combination of multiple fish tails connected in series with different waveforms to make the overall fish tail show a fluctuating forward performance.

3.1 Drive Mode

The soft actuator of body wave structure uses hydraulic pressure as driving power. Fig. 4 shows that four 24V gear pumps are arranged in a square in front as a hydraulic source, two silicone hoses are led out from the gear pump, and each channel is used as a water pumping or draining channel. The Arduino board controls the output voltage of the L298N driver module to alternate sine waves, thereby controlling the pumping and draining processes of the four pumps in a sine pattern. Through the phase control of the waveform of

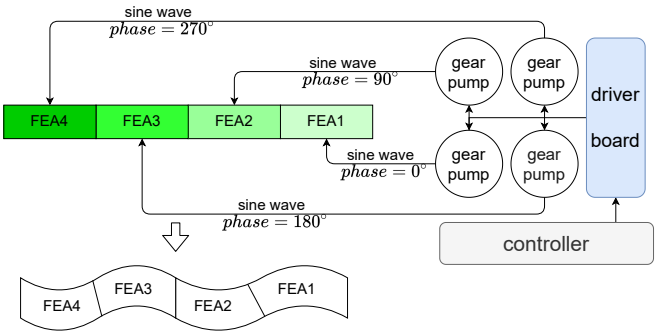

Fig. 4: Connection diagram of four-section series soft fishtail and gear pump drive.

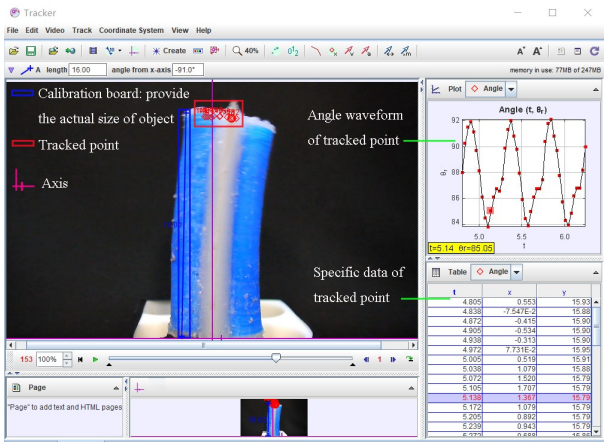

Fig. 5: Software-tracker used in experiments.

the pumping and drainage process, the alternating swing of four fish tails can be realized.

3.2 Waveform Analysis

The swing phase, frequency and amplitude of each fish tail determine the overall fish tail swing waveform, which in turn is determined by the output control signal waveform of the controller. In order to make the fish tail swing more controllable, we keep the swing frequency and amplitude of each section of fish tail equal. However, due to craftsmanship, the physical characteristics of each actuator are different. Therefore, it's necessary to explore how the pressure of each actuator change under specified swing frequency and amplitude. Then we change the swing phase of each fish tail, for example: $(0°, 45°, 90°, 135°)$ $(0°, 90°, 180°, 270°)$ $(0°, 60°, 120°, 180°)$, to observe the waveform of the entire fish tail swing.

4 Experiment

This experiment is to explore the characteristics of FEAs. For every FEA, the production methods and materials used for FEAs are the same. Due to the accuracy of the mold and manufacturing process, the dynamic characteristics of each FEA are not exactly the same, but they are largely the same, which means that the factors affecting their dynamic characteristics are similar. Therefore, this experiment only gives the detailed analysis of one FEA.

4.1 Preparation

In this experiment, we change the amplitude and phase of the input sine wave to explore the maximum swing angle and swing frequency of FEA. It should be noted that the output voltage of the power supply is not the standard power supply voltage and has a certain error. For example, actual output voltage of the 12V power supply used is 11V, and the actual output voltage of the 24V power supply is 21.67V. Therefore, it is necessary to pay attention to actual output voltage when adjusting the duty cycle of PWM.

4.2 Typical Waveform Analysis

Software-tracker (Fig. 5) is adopted to collect data. We input the scale and select tracking point at first, then the manual or automatic tracking is performed to obtain desired angle waveform.

The frequency of the tail swing controls the speed and style the fish swimming. Moreover, the difference in the swing frequency of each fish tail section can also enable the fish to achieve complex motion patterns such as turning. The input signal of the water pump can be divided into two variables: voltage amplitude and voltage period. If the voltage amplitude changes while the voltage period is constant, the swing frequency is basically unchanged. As shown in Fig. 6(a), regardless of the voltage amplitude is 8V 11V or 15V, the swing frequency is 0.67V. If the voltage period becomes larger while the voltage amplitude is constant, the swing frequency will be significantly smaller and is inversely proportional to the voltage period. As shown in Fig. 6(b), when the voltage period is 600ms, 1000ms, 1500ms, the swing frequency is 2.22Hz, 1.18Hz, 0.67Hz. Therefore, if we want to adjust the swing frequency of each fish tail, only need to adjust the frequency of the input voltage proportionally.

Due to the complex structure of the soft chamber and the characteristics of the material, the swing waveform cannot strictly follow the theoretical waveform. Next, we will analyze the influence of the input signal on the distortion of the fish tail swing.

The angle tracking trajectory(Fig. 6(b)) shows that as the voltage period increases, the waveform changes from its original smoothness to many dead zones and rebounds. Comparing the brake with smaller curvature and larger curvature, it can be clearly seen that when the brake is bent to a greater degree, the contraction of the inner chamber is very serious, which makes its braking characteristics distorted severely. i.e., many dead zones and rebounds appear.

According to the above analysis, as the input voltage cycle increases, the waveform distortion will become larger, but it will be different under different input voltage amplitudes. As the input voltage amplitude increases, the waveform of the brake swing is getting smoother. It is shown in the Fig. 6(a), the smoothness of the waveform is different at different voltage amplitude while keeping the time period constant at 1600ms. In the above observation, when the input voltage crosses the zero point or the brake reaches the maximum bending state, the waveform is most likely distorted. And as the amplitude of the input voltage becomes larger, the slope at the zero point of the waveform becomes larger, resulting in a faster moving away from the zero range, Therefore, if the input voltage amplitude is large enough, the input waveform can leave the zero point before the distortion

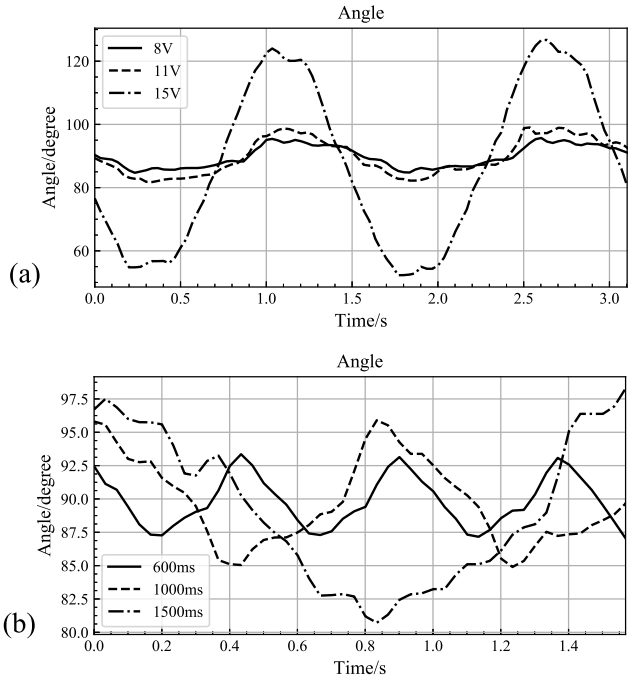

Fig. 6: (a) the input voltage cycle is 1600ms, and the amplitude gradually increases; (b) the input voltage amplitude is 10V, and the period gradually increases.

appears.

If the distortion voltage threshold of the vibration waveform is m, the input voltage frequency is ω, and the input voltage amplitude is A, the relationship between the range of the distortion time and the distortion threshold can be expressed as:

$$A \sin(\omega t) < m \tag{1}$$

The range of the distortion time can be expressed as:

$$t < 2\frac{\sin^{-1}\left(\frac{m}{A}\right)}{\omega} \tag{2}$$

As A increases, the range of distortion time gradually shrinks. When A is greater than 15V, the motion can present a smooth sinusoidal waveform.

4.3 Maximum Deflection Angle Analysis

No matter the left or right angle, the maximum deflection angle always increases as the amplitude and period of the input voltage increase. According to the relationship between the input voltage and the pumping of the gear pump, the conversion water volume of the left and right chambers in a half cycle is calculated by the following formula:

$$\int_0^{\frac{\pi}{\omega}} A \sin(\omega t)\, dt = \frac{2A}{\omega} = 2AT \tag{3}$$

Therefore, as the voltage period and amplitude increase, the theoretical conversion water volume increases. However, it is unreliable to use mathematical formulas to model the conversion of the water volume and the bending angle of the brake. By observing the experimental results (as shown in Fig. 7(a)), there is a positive correlation between them with saturation and dead zone non-linear relationship.

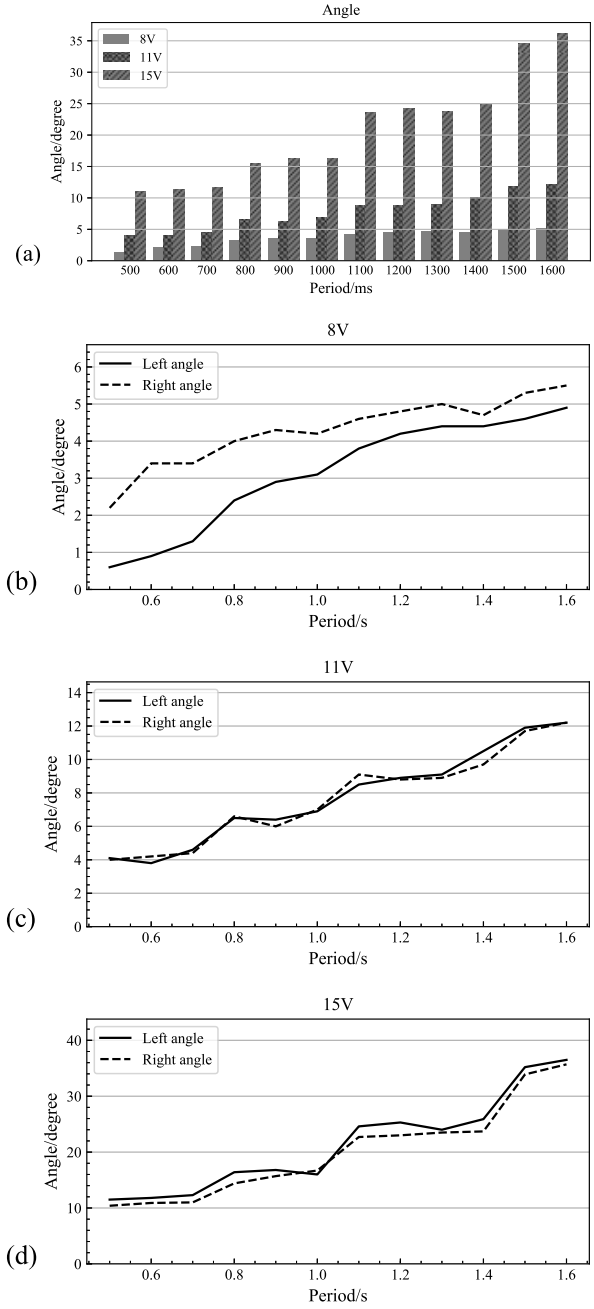

Fig. 7: (a) The Maximum angle varies with the input voltage amplitude and period; (b) (c) (d) Maximum deflection angle of different input voltage amplitude.

Observing the change of the left and right maximum bending angle as the period becomes larger when the input amplitude is 15V, we find two obvious plateaus: $T = 500ms \sim 700ms$ and $T = 1100ms \sim 1400ms$. First, when $T = 500ms \sim 700ms$, the vibration amplitude of the brake is very small, so the speed of the change with the cycle is relatively slow. When $T = 1100ms \sim 1400ms$, the amplitude of the brake will enter a bottleneck for some time, until T to $1500ms$, a step increase appears.

Generally speaking, at the same input voltage amplitude, the maximum deflection angle of the brake is positively correlated with the input voltage period.

The above analysis shows the relationship between the maximum deflection angle and the period of the input volt-

age, but what is the difference between such a curve under different input voltage amplitudes. By observing Fig. 7 (b) (c) (d), the following conclusions are drawn. The first is the plateaus characteristics obtained from the above analysis. As the input voltage increases, the appearance of the platform specificity will become more obvious, but when $U = 8V$, there will be no obvious platform characteristics. Secondly, when $U = 8V$, there is a strange phenomenon that the maximum deflection angle to the left is always greater than the maximum deflection angle to the right. After repeated comparison experiments, we find that the initial water filling volume of the left and right chambers cannot be consistent. If the input voltage is large enough or the voltage cycle is large enough, the exchange water volume is much higher than the initial phase difference between the two chambers. The impact will be small.

When the input voltage is too small, the exchange water volume when the brake swings from side to side is small, so the asymmetry of the water volume in the two chambers at the initial moment has big influence, leading to the final difference in the maximum deflection angle between the left and right sides

5 Conclusion

In this paper, some existing soft robot fish designs are summarized, and based on the previous work, a design and manufacturing scheme of an eel-like soft robotic fish driven by four fiber-reinforced FEAs is proposed. This paper describes in detail the design of the fish head which is responsible for the movement control and the power supply of the fish and the structure of the tail which is composed of four soft actuators. Using gear pump as power source, the drive circuit and generation of controlling voltage signal is also carefully considered. In this paper, we provide a complete fabrication process of the whole design implementation. The experiment illustrates the feasibility of simulating the eel's flexible underwater movement as well as superiority of the applying soft structures in bionics.

References

[1] A. D. Marchese, C. D. Onal, and D. Rus, Autonomous Soft Robotic Fish Capable of Escape Maneuvers Using Fluidic Elastomer Actuators, *Soft Robot.*, 1(1): 75–87, 2014.

[2] M. T. Tolley, R. F. Shepherd, and M. Karpelson, An untethered jumping soft robot, *IEEE Int. Conf. Intell. Robot. Syst.*, 2014: 561–566.

[3] H. Lipson, Challenges and Opportunities for Design, Simulation, and Fabrication of Soft Robots, *Soft Robot.*, 1(1): 21–27, 2014.

[4] J. Hiller, and H. Lipson, Automatic design and manufacture of soft robots, *IEEE Trans. Robot.*, 28(2): 457–466, 2012.

[5] Y. Sun, M. Li, and M. H Ang Jr, Fiber Pattern Optimization for Soft Robotic Pad, *Extreme Mechanics Letters*, 41:101055, 2020.

[6] Y. Sun, M. Li, and H. Feng, Soft Robotic Pad Maturing for Practical Applications, *Soft Robotics*, 7(1): 30-43, 2020.

[7] Y. Sun, J. Guo, and T. M. Miller-Jackson, Design and fabrication of a shape-morphing soft pneumatic actuator: Soft robotic pad, *2017 IEEE/RSJ International Conference on Intelligent Robots and Systems (IROS)*, 2017: 6214-6220.

[8] H. Lipson, and M. Kurman, *Fabricated: The New World of 3D Printing*. Hoboken: Wiley, 2013, chapter 1.

[9] J. G. Cham, S. A. Bailey, and J. E. Clark, Fast and robust: Hexapedal robots via shape deposition manufacturing. *Int. J. Rob. Res.*, 21(10): 869–882, 2002.

[10] Y. Xia and G. M. Whitesides, Soft lithography, *Angew. Chemie - Int. Ed.*, 37(5): 550–575, 1998.

[11] E. Brown, N. Rodenberg, and J. Amend, Universal robotic gripper based on the jamming of granular material, *Proc. Natl. Acad. Sci. U. S. A.*, 107(44): 18809–18814, 2010.

[12] A. D. Marchese, K. Komorowski, and C. D. Onal, Design and control of a soft and continuously deformable 2D robotic manipulation system, *Proc. - IEEE Int. Conf. Robot. Autom.*, 2014: 2189–2196.

[13] N. Napp, B. Araki, and M. T. Tolley, Simple passive valves for addressable pneumatic actuation, *Proc. - IEEE Int. Conf. Robot. Autom.*, 2014: 1440–1445.

[14] R. K. Katzschmann, J. DelPreto, and R. MacCurdy, Exploration of underwater life with an acoustically controlled soft robotic fish, *Sci. Robot.*, 3(16): 1–13, 2018.

[15] M. Wehner, R. L. Truby, and D. J. Fitzgerald, An integrated design and fabrication strategy for entirely soft, autonomous robots, *Nature*, 536(7617): 451-455, 2016.

[16] Y. Zhang, Z. Li, and Y. Du, Closed-Loop Pitch Attitude Control of Biomimetic Robotic Fish, *IEEE 9th Data Driven Control and Learning Systems Conference*, 2020: 1193-1197.

[17] A. J. Ijspeert, Central pattern generators for locomotion control in animals and robots: a review, *Neural Networks*, 21(4): 642-653, 2008.

[18] H. Feng, Y. Sun, and P. A. Todd, Body Wave Generation for Anguilliform Locomotion Using a Fiber-Reinforced Soft Fluidic Elastomer Actuator Array Toward the Development of the Eel-Inspired Underwater Soft Robot, *Soft Robotics*, 7(2): 233-250, 2020.

[19] Y. Sun, H. K. Yap, and X. Liang, Stiffness Customization and Patterning for Property Modulation of Silicone-Based Soft Pneumatic Actuators, *Soft Robotics*, 4(3): 251-260, 2017.

[20] Y. Sun, X. Liang, and H. K. Yap, Force measurement toward the instability theory of soft pneumatic actuators, *IEEE Robotics and Automation Letters*, 2(2): 985-992, 2017.

[21] Y. Sun, S. Song, and X. Liang, A miniature soft robotic manipulator based on novel fabrication methods, *IEEE Robotics and Automation Letters and ICRA 2016*, 1(2): 617-623, 2016.